Hydrodynamic Modeling of Gas/Particle Flows in Riser Reactors

J. J. Nieuwland, M. van Sint Annaland, J. A. M. Kuipers, and W. P. M. van Swaaij
Dept. of Chemical Engineering, Twente University of Technology, 7500 AE Enschede, The Netherlands

Complex hydrodynamic behavior of circulating fluidized beds makes their scale-up very complicated. In particular, large-scale lateral solids segregation causes a complex two-phase flow pattern which influences significantly their performance. Lateral solids segregation has been attributed to direct collisional interactions between particles as well as to interaction between gas-phase eddies and dispersed particles. However, these phenomena have not been investigated thoroughly.

This article discusses an advanced 2-D hydrodynamic model developed for circulating fluidized beds based on the two-fluid concept. Because theory to model the interaction between gas-phase eddies and dispersed particles is not available, turbulence was modeled on a macroscopic scale using a modified Prandtl mixing length model. To model the influence of direct particle-particle collisions the kinetic theory for granular flow was applied based on the Chapman-Enskog theory of dense gases. For model validation purposes, a cold flow circulating fluidized bed was employed in which sand was transported with air as fluidizing agent. The column is equipped with pressure transducers to measure the axial pressure profile and with a reflective optical fiber probe to measure the local solids concentration and axial solids velocity. Theoretically calculated solids concentration and axial solids velocity agree satisfactorily with experiment, especially when one realizes that the model contains no adjustable parameters. In general, however, the model slightly underpredicted the experimentally observed lateral solids segregation and yielded a more peaked velocity profile compared to its experimental counterpart.

Introduction

Despite the fact that circulating fluidized beds (CFBs) find a widespread application in the chemical and process industries for several decades (Yerushalmi and Avidan, 1985), their design and scale-up is still very difficult which is mainly due to the complex hydrodynamic behavior.

Experimental investigations have clearly demonstrated that the solids distribution in these systems is inhomogeneous in both axial and radial directions (Kwauk et al., 1986; Bader et al., 1988; Dry, 1986; Miller and Gidaspow, 1992). The inhomogeneous solids distribution in the axial direction can be attributed to the acceleration of particles which enter the column at the bottom of the bed with low velocity. The inhomogeneous solids distribution in the radial direction, which is unfortunately less well understood, may cause significant downflow of particles near the tube wall. The nonuniform solids distribution and solids flow influences the particle resi-

dence-time distribution, and thereby the reactor performance, to a large extent. Understanding and (a-priori) prediction of the complex hydrodynamic behavior is of crucial importance for developing processes involving CFBs.

For the lateral segregation two mechanisms have been proposed in literature: mutual particle interactions (Sinclair and Jackson, 1989; Ding and Gidaspow, 1990) and interaction between particles and turbulent gas-phase eddies (Berker and Tulig, 1986; Louge et al., 1991). The first mentioned mechanism has been studied among others by Sinclair and Jackson (1989). They developed a 1-D hydrodynamic model which describes the particle concentration and the velocities of both phases for fully developed flow as a function of the radial coordinate. These authors succeeded in predicting a nonuniform radial solids distribution only if some terms were omitted in the adopted collisional theory. Louge et al. (1991) used a similar model, which additionally incorporates a simple turbulence model to describe the interaction between particles

and turbulent gas-phase motion on a microscopic scale. They were able to solve the complete equation for the collisional theory (i.e., without omitting certain terms). Since the model of Louge et al. is only valid for very dilute flows ($< 0.5\%$) no solids segregation was predicted. The calculated velocity profiles agreed well with selected experimental data reported by Tsuji et al. (1984), indicating the importance of turbulence modeling.

The present work is concerned with the further development of an advanced hydrodynamic model which is based on the two-fluid concept (Kuipers, 1990). Previous studies have shown that gas bubble behavior in fluidized beds can be predicted satisfactorily by this model without the use of any fitted parameters (Kuipers et al., 1991). In the present study the wider applicability of the model to predict key hydrodynamic features of CFBs will be investigated. A simple turbulence model has been incorporated in the original model to describe the macroscopic turbulence behavior in the gas phase. In addition the collisional interaction between the particles has been modeled, using the kinetic theory of granular flow based on the Chapman-Enskog theory of dense gases.

Two-Fluid Model
Governing equations

In principle the hydrodynamics of dense gas-solid two-phase flow may be described by the Newtonian equations of motion for each suspended particle and the Navier Stokes equations for the gas phase. However, due to the huge number of particles the number of resulting equations is far too high to permit direct solution on present (super-) computers. Therefore, the particulate phase is also considered as a continuous medium which can be justified due to the very high particle concentration in the systems of interest (Anderson and Jackson, 1967). The nonstationary continuity and momentum equations are given by:

Continuity Equation Gas Phase:

$$\frac{\partial}{\partial t}(\epsilon_f \rho_f) + \frac{\partial}{\partial r} \cdot (\epsilon_f \rho_f u) = 0 \qquad (1)$$

Continuity Equation Solid Phase:

$$\frac{\partial}{\partial t}(\epsilon_s \rho_s) + \frac{\partial}{\partial r} \cdot (\epsilon_s \rho_s v) = 0 \qquad (2)$$

Momentum Equation Gas Phase:

$$\frac{\partial}{\partial t}(\epsilon_f \rho_f u) + \frac{\partial}{\partial r} \cdot (\epsilon_f \rho_f uu)$$
$$= - \epsilon_f \frac{\partial}{\partial r} P - \beta(u - v) - \frac{\partial}{\partial r} \cdot (\epsilon_f s_f) + \epsilon_f \rho_f g \qquad (3)$$

Momentum Equation Solid Phase:

$$\frac{\partial}{\partial t}(\epsilon_s \rho_s v) + \frac{\partial}{\partial r} \cdot (\epsilon_s \rho_s vv)$$
$$= - \epsilon_s \frac{\partial}{\partial r} P + \beta(u - v) - \frac{\partial}{\partial r} \cdot (\epsilon_s s_s) + \epsilon_s \rho_s g - \frac{\partial}{\partial r} P_s \qquad (4)$$

In the solid phase momentum equation the gradient of the particulate phase pressure P_s (in $\mathrm{kg \cdot m^{-1} \cdot s^{-2}}$) can be associated with particle-particle interactions.

Due to the mathematical complexity of the set nonlinear partial differential equations, a numerical solution procedure is required (Kuipers et al., 1993). The porosity, pressure, and velocity vectors of both phases constitute the basic variables. These variables can be obtained from Eqs. 1–4 provided that constitutive equations are specified which define the remaining variables in terms of the basic variables.

Constitutive equations

The fluid density ρ_f (in $\mathrm{kg \cdot m^{-3}}$) is related to the temperature and pressure by the ideal gas law, while for the solid density ρ_s a constant value is taken.

In dense regimes (i.e., $\epsilon_f < 0.80$) the interphase momentum transfer coefficient β (in $\mathrm{kg \cdot m^{-3} \cdot s^{-1}}$) can be obtained from the well-known Ergun equation

$$\beta = 150 \frac{(1 - \epsilon_f)^2}{\epsilon_f} \frac{\mu_f}{d_p^2} + 1.75(1 - \epsilon_f) \frac{\rho_f}{d_p} |u - v| \qquad (5)$$

For $\epsilon_f \geq 0.80$, the interphase momentum transfer coefficient can be derived from the correlation of Wen and Yu (1966). Thus, in dilute regimes ($\epsilon_f \geq 0.80$), β is given by

$$\beta = \frac{3}{4} C_{d,s} \frac{\epsilon_f(1 - \epsilon_f)}{d_p} \rho_f |u - v| \epsilon_f^{-2.65} \qquad (6)$$

In this relation the drag coefficient for an isolated particle $C_{d,s}$ depends on the particle Reynolds number Re_p ($\rho_f \epsilon_f |u - v| d_p / \mu_f$) as follows (Schiller and Naumann, 1935)

$$C_{d,s} = \begin{cases} \dfrac{24}{Re_p} + \dfrac{3.6}{Re_p^{0.313}} & Re_p < 1{,}000 \\ 0.44 & Re_p \geq 1{,}000 \end{cases} \qquad (7)$$

It is assumed that the internal molecular momentum transport in the gas phase is not directly influenced by the particles, which implies that the viscous stress tensor in the gas phase s_f (in $\mathrm{kg \cdot m^{-1} \cdot s^{-2}}$) is given by

$$s_f = -\left[\left(\xi_f - \frac{2}{3} \mu_f \right)\left(\frac{\partial}{\partial r} \cdot u \right) I \right.$$
$$\left. + \left(\mu_f + \mu_f^t \right)\left(\left(\frac{\partial}{\partial r} u \right) + \left(\frac{\partial}{\partial r} u \right)^T \right) \right] \qquad (8)$$

The shear viscosity is taken as the sum of the (constant) gas-phase shear viscosity and an eddy viscosity to account for turbulent momentum transport. The eddy viscosity is given by a modified Prandtl mixing length model as follows

$$\mu_f^t = \rho_f K^2 (R - r)^2 \left| \frac{\partial u_z}{\partial r} \right| \psi(\epsilon_f) \qquad (9)$$

where the function $\psi(\epsilon_f)$ corrects for the presence of particles. For the function $\psi(\epsilon_f)$ as a first approximation, a simple linear form has been chosen which equals 1 for single-phase flow ($\epsilon_f = 1$) and 0 for flow through a bed at incipient fluidization ($\epsilon_f = \epsilon_{f,mf}$)

$$\psi(\epsilon_f) = \frac{\epsilon_f - \epsilon_{f,mf}}{1 - \epsilon_{f,mf}} \qquad (10)$$

For single-phase turbulent flow the empirical parameter K has the value 0.36 (Deissler, 1955). The internal momentum transport in the particulate phase (s_s and P_s) depends strongly on the collisional behavior of the individual particles. To describe this collisional behavior, use can be made of the kinetic theory of granular flow (KTGF), originally developed by Jenkins and Savage (1983) and Lun et al. (1984). This theory will be considered in more detail in the next section.

Kinetic theory of granular flow

In the KTGF collisional particle interaction in a granular medium is modeled following the Chapman-Enskog approach for dense gases (Chapman and Cowling, 1970). The kinetic theory of gases, however, needs to be extended for two conceptual differences.

The first difference is the possible dissipation of kinetic fluctuation energy in a granular medium during mutual particle collisions due to inelastic deformations. Furthermore, energy can be dissipated due to friction of particles with the surrounding fluid.

In the KTGF the actual particle velocity c (in m·s^{-1}) is decomposed in a local mean velocity v (in m·s^{-1}) and a superimposed random fluctuation velocity C (in m·s^{-1}). Associated with the random motion of the particles, a pseudo temperature θ can be defined

$$\frac{3}{2}\theta = \frac{1}{2}\overline{C \cdot C} \qquad (11)$$

where the overline denotes ensemble averaging.

Since the unknown transport terms s_s and P_s depend on this pseudo temperature, an additional transport equation for the kinetic energy of the random motion of the particles is required to determine the pseudo temperature distribution.

Boltzmann Integral-Differential Equation. Particle quantities (i.e., mass m (in kg), momentum of the random motion mC, and kinetic energy of the random motion $1/2\,mC^2$) can be transported by particles according to two different transport mechanisms (Figure 1). On one hand, particles can transport a quantity by carrying it during their free flight between collisions (kinetic transport). Modeling this transport mechanism requires the velocity distribution function f (in s^3·m^{-6}) of individual particles. The probable number of particles present at time t (in s) in a volume dr at position r possessing a velocity between c and $c + dc$ is represented by f (c, r; t) $dr\,dc$. The number of particles present per unit volume and the ensemble average of a particle quantity are respectively given by
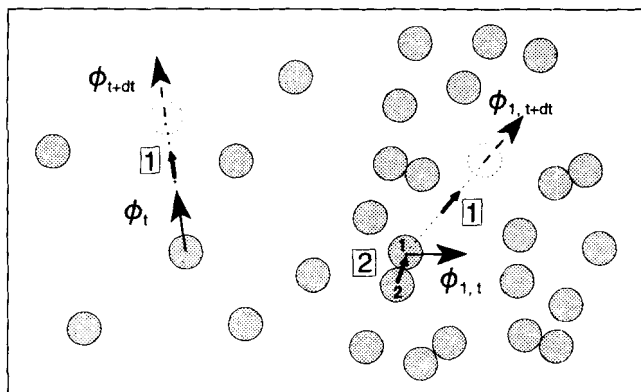
$$n = \int f(c, r; t)\, dc \qquad (12)$$

Figure 1. Transport mechanisms for quantity ϕ within the particulate phase: 1. kinetic and 2. collisional transport mode.

$$\overline{\phi} = \frac{1}{n}\int \phi f(c, r; t)\, dc \qquad (13)$$

On the other hand, particle quantities can be transferred during collisions (collisional transport). This transport mechanism is described using a pair distribution function $f^{(2)}$ (in s^3·m^{-6}). Similar to the velocity distribution function, the pair distribution function is defined such that $f^{(2)}$ (c_1, r_1; c_2, r_2; t) $dr_1\,dr_2\,dc_1\,dc_2$ represents the probability of finding a pair of particles at time t in volumes dr_1 and dr_2 centered at r_1 and r_2 having velocities between c_1 and $c_1 + dc_1$ and c_2 and $c_2 + dc_2$ respectively.

Modeling these transport mechanisms results in the well-known Boltzmann integral-differential equation (Nieuwland, 1995), in which the lefthand side originates from the kinetic transport mechanism and the righthand side emerges from collisional interactions

$$\frac{Df}{Dt} + C \cdot \frac{\partial f}{\partial r} + \frac{\partial}{\partial C}\cdot(Ff) - \frac{Dv}{Dt}\cdot\frac{\partial f}{\partial C} - \frac{\partial f}{\partial C}C:\frac{\partial}{\partial r}v$$

$$= \int\int\{f^{(2)}(c', r; c'_1, r + d_p k; t)$$

$$- f^{(2)}(c, r; c_1, r - d_p k; t)\}d_p^2(c_{12}\cdot k)dk\,dc_1 \qquad (14)$$

In this equation c' (in m·s^{-1}) denotes the particle velocity after a collision, which can be related to the particle velocity prior to collision by a coefficient of restitution e, as indicated by Jenkins and Savage (1983). A value $e = 1$ implies fully elastic collisions, while smaller values give rise to energy dissipation due to inelastic deformations.

Maxwell Transport Equation. Multiplying the Boltzmann equation with a particle quantity ϕ and integrating over all possible velocities yields the general Maxwell transport equation

$$\frac{D(n\overline{\phi})}{Dt} + n\overline{\phi}\frac{\partial}{\partial r}\cdot v + \frac{\partial}{\partial r}\cdot n\overline{\phi C} - n\left\{\overline{\frac{D\phi}{Dt}} + \overline{C\cdot\frac{\partial\phi}{\partial r}}\right.$$

$$\left. + \overline{F\cdot\frac{\partial\phi}{\partial C}} - \overline{\frac{Dv}{Dt}\cdot\frac{\partial\phi}{\partial C}} - \overline{\frac{\partial\phi}{\partial C}C:\frac{\partial}{\partial r}v}\right\} = \frac{\partial}{\partial r}\cdot\theta_c(C + v)$$

$$+ \chi_c(C + v) \qquad (15)$$

where

$$\theta_c(\phi(c)) = -\frac{d_p^3}{2} \iiint_{c_{12} \cdot k > 0} (\phi' - \phi)(c_{12} \cdot k)k$$

$$\times \left\{ 1 - \frac{1}{2!}\left(d_p k \cdot \frac{\partial}{\partial r}\right) + \frac{1}{3!}\left(d_p k \cdot \frac{\partial}{\partial r}\right)^2 + \dots \right\} f^{(2)}(c, r$$

$$- d_p k; c_1, r; t) dk dc dc_1 \quad (16)$$

$$\chi_c(\phi(c)) = \frac{d_p^2}{2} \iiint_{c_{12} \cdot k > 0} (\phi_1' + \phi' - \phi_1 - \phi)(c_{12} \cdot k)$$

$$f^{(2)}(c, r - d_p k; c_1, r; t) dk dc dc_1 \quad (17)$$

c_{12} is the relative velocity of particle 1 to particle 2 (in $m \cdot s^{-1}$); θ_c and χ_c are collisional integrals. The Maxwell equation describes the transport of an ensemble averaged particle quantity $\overline{\phi}$ by kinetic and collisional transport mechanisms. As demonstrated by Ding and Gidaspow (1990), taking $\phi = m$ and $\phi = mC$ in Eq. 15 results in the particulate phase continuity Eq. 2 and the particulate phase momentum Eq. 4 respectively. Substituting the kinetic energy associated with the random motion of the particles ($\phi = 1/2mC^2$) results in a transport equation for the kinetic fluctuation energy

$$\frac{3}{2}\left\{ \frac{\partial}{\partial t}(\epsilon_s \rho_s \theta) + \frac{\partial}{\partial r} \cdot (\epsilon_s \rho_s v\theta) \right\} = -(P_s I + \epsilon_s s_s) : \frac{\partial}{\partial r}v$$

$$- \frac{\partial}{\partial r} \cdot (\epsilon_s h) + \beta(\overline{C_f \cdot C} - 3\theta) - \gamma \quad (18)$$

The two terms in the lefthand side of Eq. 18 represent respectively the accumulation and convection of kinetic fluctuation energy. On the righthand side in Eq. 18, the first term describes the production of kinetic fluctuation energy due to irreversible deformation of the velocity field. The second term models the conductive transport of kinetic fluctuation energy. The third term represents the exchange of fluctuation energy due to interphase momentum transport. The last term describes the fluctuation energy dissipation due to inelastic particle-particle interactions. In the transport equations the following transport quantities have been defined

$$p = p^k + p^c = P_s I + \epsilon_s s_s$$

$$p^k = nm\overline{CC}$$

$$p^c = \theta_c(mC) \quad (19)$$

$$q = q^k + q^c = \epsilon_s h$$

$$q^k = \frac{1}{2}nm\overline{C^2 C}$$

$$q^c = \theta_c\left(\frac{1}{2}mC^2\right) \quad (20)$$

$$\gamma = -\chi_c\left(\frac{1}{2}mC^2\right) \quad (21)$$

For evaluation of these quantities, explicit functions for the velocity distribution function f and the pair distribution function $f^{(2)}$ are required.

Velocity Distribution Function and Pair Distribution Function. Following Enskog (Chapman and Cowling, 1970), the pair distribution function is approximated by a product of two single-particle velocity distribution functions and a correction function g, the radial distribution function

$$f^{(2)}(c, r - d_p k; c_1, r_1; t)$$

$$= g\left(r - \frac{1}{2}d_p k\right) f(c, r - d_p k; t) f(c_1, r_1; t) \quad (22)$$

The radial distribution function corrects the probability of a collision for the effect of the covolume of the particles (the volume occupied by the particles). Because only slightly inelastic collisions are considered, it is assumed that collisional anisotropy will be of little importance (Jenkins and Savage, 1983). The radial distribution function then only depends on the solidity. A simple equation to fit simulation data of Alder and Wainwright (1960) has been proposed by Ogawa et al. (1980)

$$g = \frac{1}{1 - \left(\frac{\epsilon_s}{\epsilon_{s,max}}\right)^{1/3}} \quad (23)$$

in which the maximum solids concentration $\epsilon_{s,max}$ equals to 0.65.

Ding and Gidaspow (1990) suggested multiplying this equation by 0.6 to improve the agreement of the radial distribution function with simulation data for higher solidities. However, using this correction, the radial distribution function does not approach 1 for dilute systems (i.e., risers) which is inconsistent with the definition of the radial distribution function.

To our knowledge, the equation which produces the best fit of the simulation data of Alder and Wainwright has been presented by Ma and Ahmadi (1986)

$$g = 1 + 4\epsilon_s \left[\frac{1 + 2.5000\epsilon_s + 4.5904\epsilon_s^2 + 4.515439\epsilon_s^3}{\left[1 - \left(\frac{\epsilon_s}{\epsilon_{s,max}}\right)^3\right]^{0.67802}} \right] \quad (24)$$

in which the maximum solids concentration equals 0.64356.

Using the Enskog approximation for the pair distribution function, the Boltzmann Eq. 14 can be solved to obtain the velocity distribution function. Chapman and Enskog have presented an analytical iterative method to solve this integral-differential equation assuming that the frequency of mutual particle collisions is high, resulting in a small deviation from steady-state equilibrium conditions. The Chapman Enskog theory yields the velocity distribution as a power-series of the reciprocal density. The complexity of higher-order terms increases rapidly, which makes a quick convergence of the series a necessity.

Table 1. Transport Properties from a Zeroth- and First-Order Solution of the Boltzmann Equation

	Zeroth-Order Terms	First-Order Terms
p^k	$\epsilon_s \rho_s \theta I$	$-\dfrac{2\epsilon_s \mu_s^k}{\epsilon_s g}\left(1+\dfrac{8}{5}\epsilon_s g\right)\overline{\overline{\dfrac{\overset{\circ}{\partial}}{\partial r}v}}$
p^c	$2(1+e)g\epsilon_s^2 \rho_s \theta I$	$-2\epsilon_s \mu_s^c \overline{\overline{\dfrac{\overset{\circ}{\partial}}{\partial r}v}} \quad -\epsilon_s \xi_s(\dfrac{\partial}{\partial r}\cdot v)I$
		$-\dfrac{2\epsilon_s \mu_s^k}{\epsilon_s g}\dfrac{8}{5}\dfrac{(1+e)}{2}\epsilon_s g\left(1+\dfrac{8}{5}\epsilon_s g\right)\overline{\overline{\dfrac{\overset{\circ}{\partial}}{\partial r}v}}$
p^{tot}	$P_s I$	$-2\epsilon_s \mu_s^c \overline{\overline{\dfrac{\overset{\circ}{\partial}}{\partial r}v}} \quad -\epsilon_s \xi_s(\dfrac{\partial}{\partial r}\cdot v)I$
		$-\dfrac{2\epsilon_s \mu_s^k}{\epsilon_s g}\left(1+\dfrac{8}{5}\dfrac{(1+e)}{2}\epsilon_s g\right)\left(1+\dfrac{8}{5}\epsilon_s g\right)\overline{\overline{\dfrac{\overset{\circ}{\partial}}{\partial r}v}}$
q^k	0	$-\dfrac{\epsilon_s \kappa^k}{\epsilon_s g}\left(1+\dfrac{12}{5}\epsilon_s g\right)\dfrac{\partial}{\partial r}\theta$
q^c	0	$-\epsilon_s \kappa^c \dfrac{\partial}{\partial r}\theta - \dfrac{\epsilon_s \mu^k}{\epsilon_s g}\dfrac{12}{5}\dfrac{(1+e)}{2}\epsilon_s g\left(1+\dfrac{12}{5}\epsilon_s g\right)\dfrac{\partial}{\partial r}\theta$
q^{tot}	0	$-\epsilon_s \kappa^c \dfrac{\partial}{\partial r}\theta - \dfrac{\epsilon_s \kappa^k}{\epsilon_s g}\left(1+\dfrac{12}{5}\dfrac{(1+e)}{2}\epsilon_s g\right)\left(1+\dfrac{12}{5}\epsilon_s g\right)\dfrac{\partial}{\partial r}\theta$
γ	$3(1-e^2)\epsilon_s^2 \rho_s \theta g\left(\dfrac{4}{d_p}\left(\dfrac{\theta}{\pi}\right)^{1/2}\right)$	$-3(1-e^2)\epsilon_s^2 \rho_s \theta g\left(\dfrac{\partial}{\partial r}\cdot v\right)$

$$P_s = (1+2(1+e)\epsilon_s g)\epsilon_s \rho_s \theta \qquad \mu_s^k = 1.01600\dfrac{5}{16}\dfrac{m}{d_p^2}\left(\dfrac{\theta}{\pi}\right)^{1/2} \qquad \mu_s^c = \dfrac{4}{5}\epsilon_s \rho_s d_p g(1+e)\left(\dfrac{\theta}{\pi}\right)^{1/2}$$

$$\xi_s = \dfrac{4}{3}\epsilon_s \rho_s d_p g(1+e)\left(\dfrac{\theta}{\pi}\right)^{1/2} \qquad \kappa^k = 1.02513\dfrac{75}{64}\dfrac{m}{d_p^2}\left(\dfrac{\theta}{\pi}\right)^{1/2} \qquad \kappa^c = 2\epsilon_s \rho_s d_p g(1+e)\left(\dfrac{\theta}{\pi}\right)^{1/2}$$

The zeroth-order solution to the velocity distribution function is the well-known Maxwell velocity distribution function, which describes the steady-state equilibrium condition without action of any external forces (Boltzmann's H-theorem)

$$f^{(0)} = \dfrac{n}{(2\pi\theta)^{3/2}}\exp\left(-\dfrac{C^2}{2\theta}\right) \qquad (25)$$

The first-order solution to the velocity distribution function is written as a first-order perturbation to the Maxwellian state

$$f^{(1)} = f^{(0)}(1+\Phi^{(1)}) \qquad (26)$$

where

$$\Phi^{(1)} = -\dfrac{1}{ng}\left\{\left(1+\dfrac{12}{5}\epsilon_s g\right)\sqrt{2\theta}A(\mathbb{C})C\cdot\dfrac{\partial}{\partial r}\ln(\theta)\right.$$
$$\left.+2\left(1+\dfrac{8}{5}\epsilon_s g\right)B(\mathbb{C})C^0 C:\dfrac{\partial}{\partial r}v\right\} \qquad (27)$$

($\mathbb{C}$ is the dimensionless fluctuation velocity $(C/(2\theta)^{1/2})$. In Nieuwland (1995) it is shown in more detail how to derive the first-order perturbation function $\Phi^{(1)}$.

Having derived explicit functions for the velocity distribution function f and the pair distribution function $f^{(2)}$, the transport quantities defined in Eqs. 19–21 can be evaluated. Table 1 shows the results which have been obtained by applying the zeroth- and first-order solution of the Boltzmann

equation respectively, and additionally shows the kinetic and collisional contributions.

Rewriting p in the general form for the Newtonian stress-tensor s_s (Eq. 19)

$$s_s = -\left[\left(\xi_s - \frac{2}{3}\mu_s\right)\left(\frac{\partial}{\partial r} \cdot v\right)I + \mu_s\left(\left(\frac{\partial}{\partial r}v\right) + \left(\frac{\partial}{\partial r}v\right)^T\right)\right]$$

(28)

yields the following expressions for the particulate phase pressure P_s and the particulate phase bulk and shear viscosities [ξ_s (in $kg \cdot m^{-1} \cdot s^{-2}$) and μ_s(in $kg \cdot m^{-1} \cdot s^{-1}$)]

$$P_s = [1 + 2(1 + e)\epsilon_s g]\epsilon_s \rho_s \theta$$

(29)

$$\xi_s = \frac{4}{3}\epsilon_s \rho_s d_p g(1 + e)\sqrt{\frac{\theta}{\pi}}$$

(30)

$$\mu_s = \mu_s^c + \mu_s^k \frac{\left(1 + \frac{8}{5}\frac{(1+e)}{2}\epsilon_s g\right)\left(1 + \frac{8}{5}\epsilon_s g\right)}{\epsilon_s g}$$

(31)

in which

$$\mu_s^c = \frac{4}{5}\epsilon_s \rho_s d_p g(1 + e)\sqrt{\frac{\theta}{\pi}}$$

(32)

$$\mu_s^k = 1.01600\frac{5}{16}\frac{m}{d_p^2}\sqrt{\frac{\theta}{\pi}}$$

(33)

Rewriting the conductive transport term of the kinetic fluctuation energy q (in $kg \cdot s^{-3}$) as a Fourier type energy flux h (in $kg \cdot s^{-3}$) (Eq. 20)

$$h = -\kappa\frac{\partial}{\partial r}\theta$$

(34)

results in the following expression for the fluctuation energy conductivity κ ($kg \cdot m^{-1} \cdot s^{-1}$)

$$\kappa = \kappa^c + \kappa^k \frac{\left(1 + \frac{12}{5}\frac{(1+e)}{2}\epsilon_s g\right)\left(1 + \frac{12}{5}\epsilon_s g\right)}{\epsilon_s g}$$

(35)

where

$$\kappa^c = 2\epsilon_s \rho_s d_p g(1 + e)\sqrt{\frac{\theta}{\pi}}$$

(36)

$$\kappa^k = 1.02513\frac{75}{64}\frac{m}{d_p^2}\sqrt{\frac{\theta}{\pi}}$$

(37)

The kinetic contributions of the transport quantities (μ_s^k and κ^k) have been approximated by a fourth-order Sonine polynomial (Chapman and Cowling, 1970, p. 169).

Comparison with Results in Literature. The results which have been derived in this study on basis of the Chapman-Enskog approach are compared with the results obtained by Lun et al. (1984) and Ding and Gidaspow (1990) in Table 2.

Ding and Gidaspow (1990) adopted the Maxwell velocity distribution function (Eq. 25). Nevertheless in calculating the collision integrals appearing in Eqs. 19 to 21 they took the first-order spatial derivatives in the Taylor expansion of the velocity distribution function into account. These derivatives have been neglected in the derivation of the Maxwell velocity distribution function, according to the H-theorem of Boltzmann. This corresponds to an approach between zeroth- and first-order approximation. The relations for the particulate phase shear viscosity μ_s and the particulate phase conductivity κ derived by Ding and Gidaspow differ strongly with respect to their dependence on solids concentration compared to the relations derived in this study. These relations are compared in Figure 2 as a function of solids concentration for fully elastic particles ($e = 1$). It may be clear that for systems of interest (i.e., $\epsilon_s < 0.15$) significantly higher values for the particulate phase shear viscosity and particulate phase conductivity are obtained using the relations proposed in this work. Ding and Gidaspow incorporated only the collisional contribution in their expression for the solids phase shear viscosity, whereas the relations for the particulate phase shear viscosity and particulate phase conductivity derived in this work constitute a collisional and a kinetic part. For decreasing solids concentration, the collisional part decreases in importance due to a decrease in number of collisions, whereas the kinetic part increases considerably due to the increasing mean free path of the particles. A detailed analysis showed that for $\epsilon_s = 0.01$ the kinetic term was responsible for 97.5% of the total particulate phase shear viscosity, independent of particle properties and operation conditions. Not before $\epsilon_s \approx 0.15$ the kinetic and collisional contributions are of the same order of magnitude.

Lun et al. (1984) used a first-order approximation to the velocity distribution function in which they postulated that the perturbation function $\Phi^{(1)}$ could be represented by a linear combination of first-order gradients with respect to the variables n, v and θ. They determined the expansion coefficients using Grad's method. In contrast to the first-order perturbation function used in the kinetic theory of gases they recognized the necessity to include a term containing the gradient of n in case of slightly inelastic collisions. The same can be concluded when applying the Chapman Enskog theory (Nieuwland, 1995). For fully elastic collisions the equations for the transport quantities derived by Lun et al. equal the equations derived in this work. However, Lun et al. did not consider a velocity dependence of the external force per unit mass F (in $kg \cdot m \cdot s^{-2}$), resulting in a neglect of the exchange of fluctuation energy with the fluid phase in the transport equation for kinetic fluctuation energy (Eq. 18).
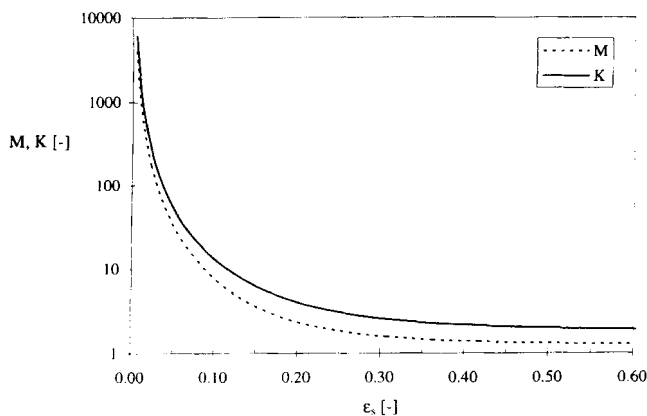
Finally, it should be noted that the expressions for the particulate phase bulk viscosity ξ_s and particulate phase pressure P_s are the same in all approaches.

Initial and boundary conditions

Initial Conditions. In all computations reported in this study the initial condition corresponds to the situation of fully developed laminar tube flow.

Table 2. Transport Quantities Derived from Chapman-Enskog, Lun et al. (1984), and Ding and Gidaspow (1990)

	Ding and Gidaspow (1990)	Lun et al. (1984)	Chapman-Enskog $(e \approx 1)$
p^k	$\epsilon_s \rho_s \theta I$	$\epsilon_s \rho_s \theta I - 2 \dfrac{\epsilon_s \mu_s^k}{\epsilon_s g} \dfrac{2}{(1+e)} \dfrac{2}{(3-e)} \left(1 + \dfrac{8}{5} \epsilon_s g \dfrac{(1+e)}{2} \dfrac{(3e-1)}{2}\right) \overset{\circ}{\overline{\dfrac{\partial}{\partial r} v}}$	$\epsilon_s \rho_s \theta I - 2 \dfrac{\epsilon_s \mu_s^k}{\epsilon_s g} \left(1 + \dfrac{8}{5} \epsilon_s g\right) \overset{\circ}{\overline{\dfrac{\partial}{\partial r} v}}$
p^c	$2(1+e) g \epsilon_s^2 \rho_s \theta I - 2 \epsilon_s \mu_s^c \overline{\dfrac{\partial}{\partial r} v} - \epsilon_s \xi_s \left(\dfrac{\partial}{\partial r} \cdot v\right) I$	$2(1+e) g \epsilon_s^2 \rho_s \theta I - 2 \epsilon_s \mu_s^c \overline{\dfrac{\partial}{\partial r} v} - \epsilon_s \xi_s \left(\dfrac{\partial}{\partial r} \cdot v\right) I$ $- 2 \dfrac{\epsilon_s \mu_s^k}{\epsilon_s g} \dfrac{2}{(3-e)} \dfrac{8}{5} (1+e) \epsilon_s g \left(1 + \dfrac{8}{5} \dfrac{(1+e)}{2} \dfrac{(3e-1)}{2} \epsilon_s g\right) \overset{\circ}{\overline{\dfrac{\partial}{\partial r} v}}$	$2(1+e) g \epsilon_s^2 \rho_s \theta I - 2 \epsilon_s \mu_s^c \overline{\dfrac{\partial}{\partial r} v} - \epsilon_s \xi_s \left(\dfrac{\partial}{\partial r} \cdot v\right) I$ $- 2 \dfrac{\epsilon_s \mu_s^k}{\epsilon_s g} \dfrac{(1+e)}{2} \dfrac{8}{5} \epsilon_s g \left(1 + \dfrac{8}{5} \epsilon_s g\right) \overset{\circ}{\overline{\dfrac{\partial}{\partial r} v}}$
q^k	0	$- \dfrac{\epsilon_s \kappa^k}{\epsilon_s g} \dfrac{2}{(1+e)} \dfrac{16}{(49-33e)} \left(1 + \dfrac{12}{5} \epsilon_s g \dfrac{(1+e)^2}{4} (2e-1)\right) \dfrac{\partial}{\partial r} \theta$	$- \dfrac{\epsilon_s \kappa^k}{\epsilon_s g} \left(1 + \dfrac{12}{5} \epsilon_s g\right) \dfrac{\partial}{\partial r} \theta$
q^c	$- \epsilon_s \kappa^c \dfrac{\partial}{\partial r} \theta$	$- \epsilon_s \kappa^c \dfrac{\partial}{\partial r} \theta - \dfrac{\epsilon_s \kappa^k}{\epsilon_s g} \dfrac{2}{(1+e)} \dfrac{16}{(49-33e)} \dfrac{16}{5} \dfrac{12}{(49-33e)} \epsilon_s g \left(1 + \dfrac{12}{5} \epsilon_s g \dfrac{(1+e)^2}{4} (2e-1)\right) \dfrac{\partial}{\partial r} \theta$ $- \epsilon_s \kappa^k \dfrac{16}{(49-33e)} \dfrac{36}{25} (e^2-1) e \dfrac{d}{d\epsilon_s} (\epsilon_s^2 g) \dfrac{\theta}{\epsilon_s} \dfrac{\partial}{\partial r} \epsilon_s$	$- \epsilon_s \kappa^c \dfrac{\partial}{\partial r} \theta - \dfrac{\epsilon_s \kappa^k}{\epsilon_s g} \dfrac{(1+e)}{2} \dfrac{12}{5} \epsilon_s g \left(1 + \dfrac{12}{5} \epsilon_s g\right) \dfrac{\partial}{\partial r} \theta$
γ	$3(1-e^2) \epsilon_s^2 \rho_s g \theta \left(\dfrac{4}{d_p} \left(\dfrac{\theta}{\pi}\right)^{1/2} - \left(\dfrac{\partial}{\partial r} \cdot v\right)\right)$	$3(1-e^2) \epsilon_s^2 \rho_s g \theta \left(\dfrac{4}{d_p} \left(\dfrac{\theta}{\pi}\right)^{1/2}\right)$	$3(1-e^2) \epsilon_s^2 \rho_s g \theta \left(\dfrac{4}{d_p} \left(\dfrac{\theta}{\pi}\right)^{1/2} - \left(\dfrac{\partial}{\partial r} \cdot v\right)\right)$

Figure 2. Particulate-phase shear viscosity μ_s and conductivity κ as a function of solids concentration ϵ_s for a restitution coefficient $e = 1$: This work vs. Ding and Gidaspow (1990).

$M = \mu_s^{\text{this work}} / \mu_s^{\text{Ding \& Gidaspow}}$; $K = \kappa^{\text{this work}} / \kappa^{\text{Ding \& Gidaspow}}$.
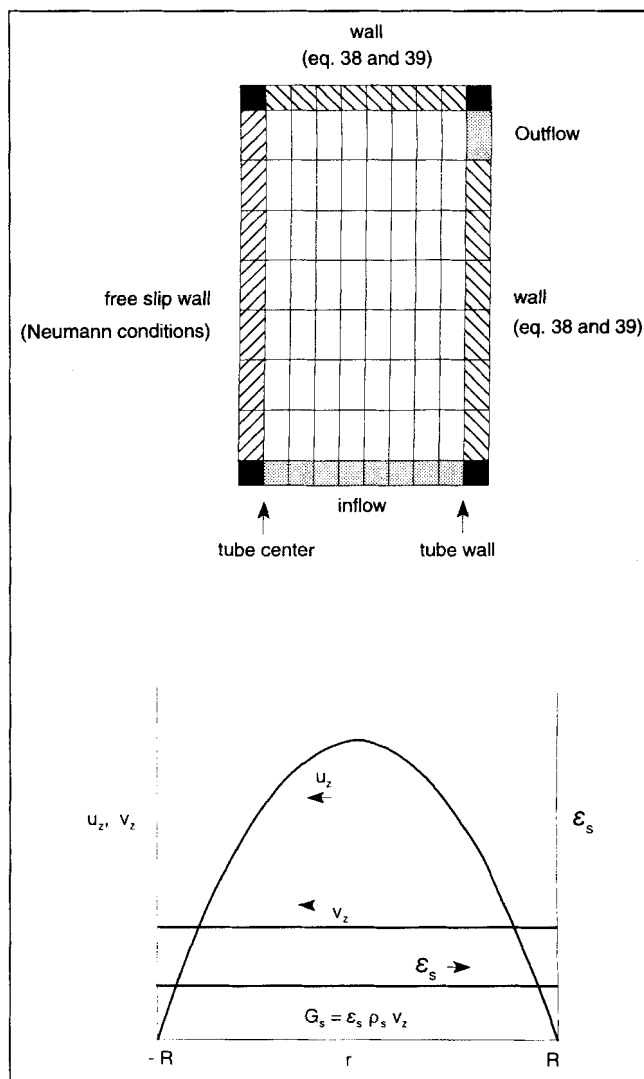
Boundary Conditions. The boundary conditions applied in the simulations are shown in Figure 3. At the bottom of the column, fluidization air enters with a parabolic velocity profile whereas the solids enter the column with a flat velocity profile. At the inflow boundary the solids volume fraction is assumed to equal the minimum fluidization solidity $\epsilon_s = 0.6$, because the solids are fed from a storage vessel kept at incipient fluidization. The solids velocity follows from the imposed solids mass flux G_s (in $\text{kg} \cdot \text{m}^{-2} \cdot \text{s}^{-1}$). The value of the granular temperature θ at inflow conditions is unknown and, therefore, as a first approximation, it is assumed that the solid-phase velocity fluctuation is of the same order of magnitude as the mean solid-phase velocity. A parametric study showed no significant influence of the inlet value of this quantity on riser hydrodynamics.

In the center of the tube, all fluxes should vanish, resulting in Neumann boundary conditions for the transport equations.

At solid walls the fluidum velocity obeys the no-slip condition, whereas the solids phase is allowed to slip along the wall. A relation for the solids velocity gradient at the tube wall has been given by Sinclair and Jackson (1989). These authors also give an expression for the pseudo Fourier fluctuation energy flux at the wall. These two boundary conditions are based on a microscopic model for particle collisions with the wall and are given by

$$- \epsilon_s \mu_s \frac{\partial v_z}{\partial r} = \frac{\rho_s \pi v_z \alpha \sqrt{\theta}}{2\sqrt{3} \left[\frac{\epsilon_{s,\max}}{\epsilon_s} - \left(\frac{\epsilon_{s,\max}}{\epsilon_s} \right)^{2/3} \right]} \quad (38)$$

$$- \kappa \frac{\partial \theta}{\partial r} = \frac{- \rho_s \pi v_z^2 \alpha \sqrt{\theta}}{2\sqrt{3} \left[\frac{\epsilon_{s,\max}}{\epsilon_s} - \left(\frac{\epsilon_{s,\max}}{\epsilon_s} \right)^{2/3} \right]}$$

$$+ \frac{\sqrt{3} \rho_s \pi (1 - e_w^2) \theta \sqrt{\theta}}{4 \left[\frac{\epsilon_{s,\max}}{\epsilon_s} - \left(\frac{\epsilon_{s,\max}}{\epsilon_s} \right)^{2/3} \right]} \quad (39)$$

Figure 3. Computational mesh and surrounding fictitious cells to incorporate boundary conditions.

In our study the values of the coefficient of restitution e_w for particle-wall collisions and the specularity coefficient α are taken as 0.9 and 0.5 respectively (Pita and Sundaresan, 1991). The formulation of the boundary conditions at the tube exit requires specific attention due to the possible occurrence of solids downflow near the tube wall. In all computations reported in this article a splash plate configuration (a horizontal plate positioned at some distance above the tube exit) has been implemented to enforce horizontal outflow of the gas solid dispersion. Computational experience has shown that the dimension of the outflow opening (i.e., the distance between the horizontal plate and the tube exit) has a negligible influence on the computed radial profiles of solids concentration and axial velocities of both phases.

Numerical solution method

The set of model Eqs. 1, 2, 3, 4 and 18, together with the constitutive equations, has been solved in 2-D axisymmetrical
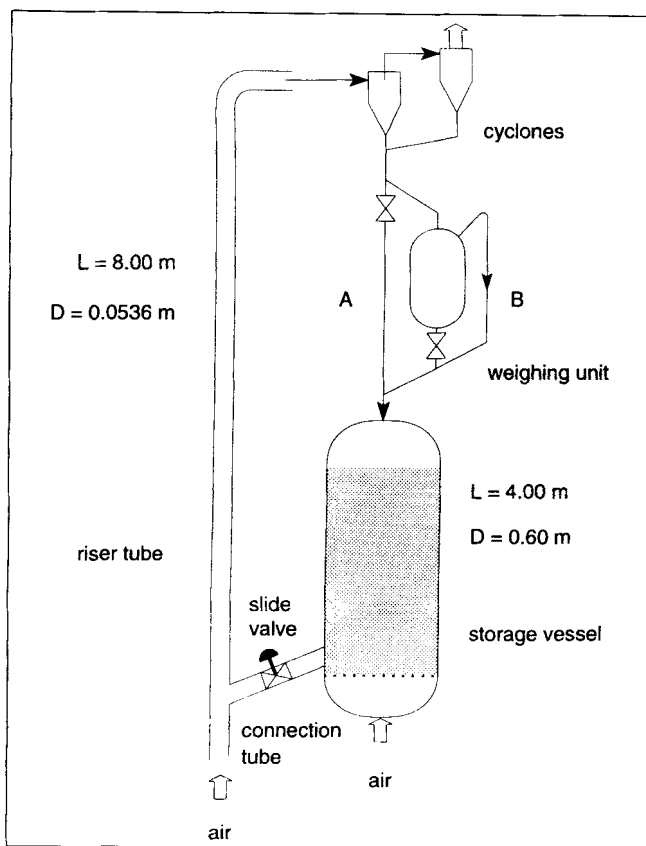
Figure 4. CFB unit.

cylindrical coordinates, using a finite-difference technique (Kuipers et al., 1993) employing a staggered grid. For evaluation of the convective transport terms the upwind scheme has been applied (Patankar, 1980). A time relaxation technique has been used to compute steady-state flow patterns, and to improve the computational efficiency a coordinate transformation has been implemented generating a coarse grid near the tube center and a fine grid near the tube wall. Typical values used for the time-step and computational cell dimensions are: $\delta t \approx 10^{-5}$ s, $\delta r \approx 1$ mm and $\delta z \approx 1$ m.

Experimental Studies

Equipment

To validate the theoretical results, the CFB hydrodynamics has been studied in a cold flow CFB unit which is shown in Figure 4. Sand particles ($W = 1,000$ kg, $d_p = 129$ μm, $\rho_s = 2,540$ kg·m^{-3}) were kept at incipient fluidization in a steel storage vessel ($L = 4.0$ m, $D = 0.6$ m) with air as fluidizing agent. The solids were fed to the riser column through a connection tube ($L = 1.0$ m, $D = 0.054$ m), mounted under 45° with respect to the riser column. The solids flux could be controlled with a slide valve, mounted in the connection tube.

Our 8-m-tall riser column made of transparent PVC has an internal diameter of 53.6 mm. Humidified air (relative humidity, 80%) was supplied at the bottom of the riser tube, to convey the solid particles.

At the exit of the riser column two cyclones separated the solid particles from the fluidizing air. The solid particles were fed back to the storage vessel after passing a weighing unit.

Experimental techniques

In axial direction 16 pressure taps were mounted in the wall of the riser column with an equidistant spacing of 47 cm. Pressure differences over these sections were measured using 2.5-m tall water manometers.

The mass-flow rate of the circulating solids could be determined by collecting the solids in the weighing unit during a certain period of time. Typically 25 kg of sand particles were collected in the weighing unit, while the gas phase was by-passed to prevent pressure buildup.

To measure both the local solids concentration and the local axial solids velocity, a reflective optical probe has been developed which is roughly based on the sample principle as the one developed by Hartge et al. (1988). To improve the quality of the signals, the mono glass fiber as used by Hartge et al. has been replaced by a bifurcated multifiber (fiber, dia. 15 μm) which eliminates the necessity to use a beam splitter. Light, emitted by a laser diode, is guided to the sensor tip by half of the glass fibers of the bifurcated multifiber. Part of the emitted light is reflected by the particles present in front of the sensor tip. This reflected light is guided by the other half of the glass fibers to a photo diode, which converts the optical signal into an electrical signal.

As Hartge et al. (1988) showed, the relation between the amplified output voltage U (V) of the photo diode and the local particle concentration is given by

$$U = U_o + a\epsilon_s^b \qquad (40)$$

In this equation U_o is the voltage signal which is obtained when no particles are present, where the value of the index b only depends on the characteristics of the particulate phase. This offers the advantageous possibility to calibrate the optical sensor in sand-water mixtures. The value of the constant a (V) follows from a measurement in a small packed bed with known bed voidage. To enable measurement of the local solids velocity the optical probe consists of two sensors with a vertical separation of 4.2 mm (Figure 5). Because the solid particles in principle pass both sensors, these sensors are expected to produce two equal voltage signals which only possess a shift in time. The time shift, obtained from cross-correlating both signals, yields the velocity of the particles moving near the probe tip. In this study measurements were performed at 13 radial positions, all at a fixed distance of 2.5 m above the solids inlet. On each position 40 measurements were made, whereas for each measurement 1,536 samples were taken with sample frequencies between 25.6 and 51.2 kHz.

Results and Discussion

For dense gas-solid systems ($\epsilon_s > 0.01$) no theory is available yet to describe the rate of production of kinetic fluctuation energy due to gas-phase turbulence (Eq. 18)

$$\overline{C_f \cdot C} \qquad (41)$$

Louge et al. (1991) modeled the correlation between the velocity fluctuations of both phases, but their treatment was restricted to very diluted flows ($\epsilon_s < 0.005$).
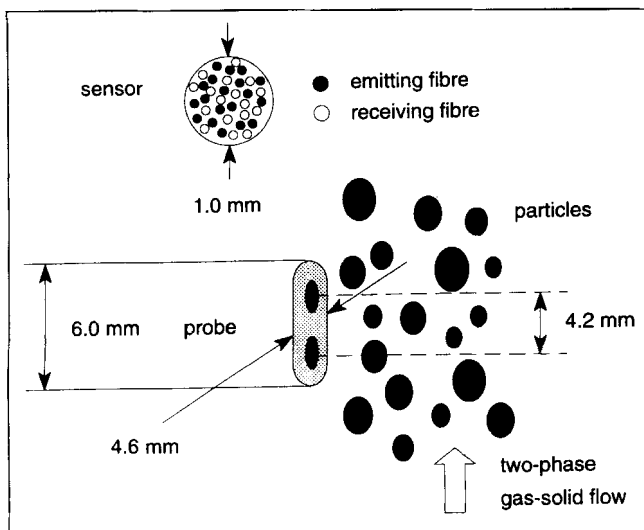
Figure 5. Optical probe containing two multifiber sensors.

Ignoring the correlation between the velocity fluctuations, the dissipation terms in the transport equation for kinetic fluctuation energy (γ and $3\beta\theta$ in Eq. 18) had to be omitted in order to solve the set of model equations derived in this work successfully. Only inelastic collisions with the wall result in a kinetic fluctuation energy loss. Corresponding to $\gamma = 0$, only fully elastic mutual particle collisions are considered ($e = 1$). Calculations with e values which slightly differ from unity (e.g., $e = 0.999$) result in extinguishment of the granular temperature and, as a consequence, fail to produce the experimentally observed lateral solids segregation. A similar strong dependence of the computed radial solids distribution with respect to the value of e has been reported by Pita and Sundaresan (1991).

In this work, it has been assumed that the rate of kinetic fluctuation energy production due to gas-phase turbulence equals the dissipation rate of kinetic fluctuation energy as a
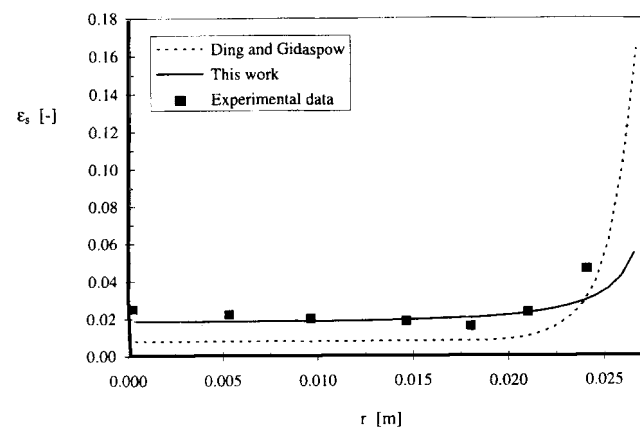
Table 3 Properties of Gas and Solids Phase Used in the Calculations

Solid Phase	Sand
Mean particle diameter, d_p	129 μm
Particle dia. distribution	$50 < d_p < 150$ μm
Particle density, ρ_s	2,540 kg·m^{-3}
Coeff. of restitution, e	1.00
Coeff. of restitution at the wall, e_w	0.90
Specularity coeff. at the wall, α	0.50
Gas Phase	Air
Operating pressure, P	1 atm
Temperature, T	20°C
Bulk viscosity, ξ_f	0.00 kg·m^{-1}·s^{-1}
Shear viscosity, μ_f	1.80×10^{-5} kg·m^{-1}·s^{-1}

result of inelastic mutual particle collisions and friction with the mean gas-phase velocity field. The same assumption has been made by Sinclair and Jackson (1989) and Pita and Sundaresan (1991, 1993), who used the expressions proposed by Lun et al. (1984).

Figure 6 shows a comparison between the theoretically calculated and experimentally determined radial solids concentration profile for a superficial gas velocity of 14.4 m·s^{-1} and a solids flux of 350 kg·m^{-2}·s^{-1} at 2.5 m above the solids inlet ($L = 8$ m, $D = 0.054$, properties of gas and solids phase are summarized in Table 3). In addition, Figure 7 shows the radial profiles for the axial solids velocity. In these figures theoretical results are shown for steady-state developed flow using the constitutive relations for μ_s and κ derived by Ding and Gidaspow (1990) and the relations derived in this work, with and without accounting for turbulence respectively. For steady state, fully developed flow the velocities of both phases and the solids concentration do not change in axial direction and in addition radial velocities equal zero. With these assumptions, the reduced momentum equations prescribe constant fluid-phase and particulate-phase pressure over the tube radius, a requirement which was met by the calculated results. From Figure 6, it follows that both hydrodynamic models predict, in accordance with experimental data, marked ra-

Figure 6. Calculated and experimentally determined solids concentration as a function of the radial position at 2.5 m above the solids entry.

$R = 0.027$ m, $u^o = 14.4$ m·s^{-1}, $G_s = 350$ kg·m^{-2}·s^{-1}, $d_p = 129$ μm, $\rho_s = 2,540$ kg·m^{-3}.
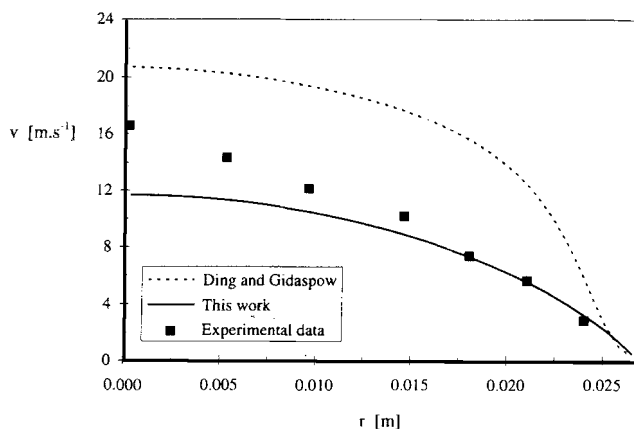
Figure 7. Calculated and experimentally determined axial solids velocity as a function of the radial position at 2.5 m above the solids entry.

$R = 0.027$ m, $u^o = 14.4$ m·s^{-1}, $G_s = 350$ kg·m^{-2}·s^{-1}, $d_p = 129$ μm, $\rho_s = 2,540$ kg·m^{-3}.
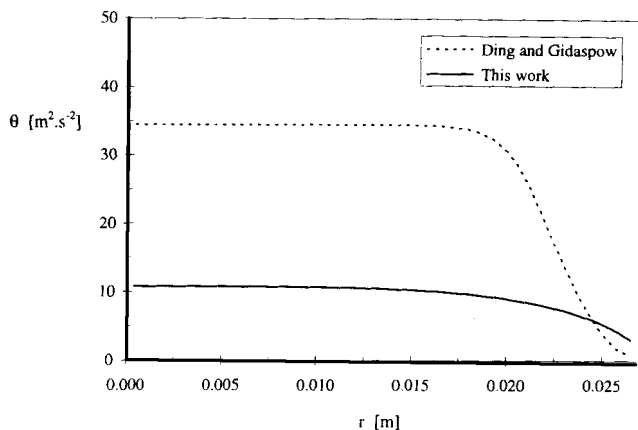
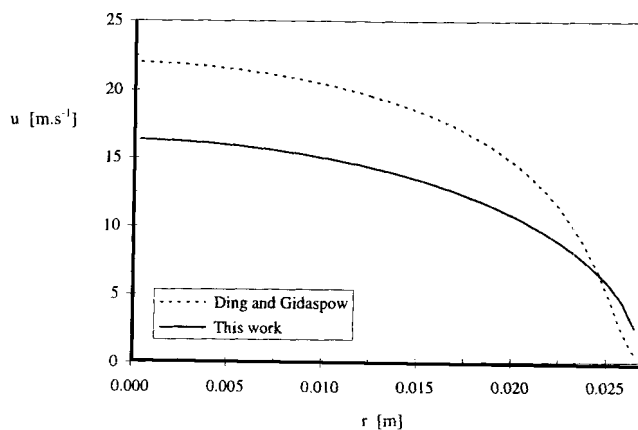**Figure 8. Calculated pseudo temperature as a function of the radial position at 2.5 m above the solids entry.**

$R = 0.027$ m, $u^o = 14.4$ m·s^{-1}, $G_s = 350$ kg·m^{-2}·s^{-1}, $d_p = 129$ μm, $\rho_s = 2,540$ kg·m^{-3}.

Figure 9. Calculated gas velocity in axial direction as a function of the radial position at 2.5 m above the solids entry.

$R = 0.027$ m, $u^o = 14.4$ m·s^{-1}, $G_s = 350$ kg·m^{-2}·s^{-1}, $d_p = 129$ μm, $\rho_s = 2,540$ kg·m^{-3}.

dial segregation. Computations in which the collisional interaction between the particles was not represented failed to describe the observed lateral solids segregation (Nieuwland et al., 1994). However, as evident from Figure 6, the hydrodynamic model using the relations proposed by Ding and Gidaspow underpredicts the experimentally observed solids concentration over the entire tube radius almost by a factor 2. As expected on basis of these results, their model overpredicts the experimentally observed axial solids velocity shown in Figure 7 to satisfy the imposed solids mass flux.

The radial solids concentration profile calculated with the model using the relations proposed in this work are in good quantitative agreement, although the model seems to underpredict the lateral solids segregation slightly. The underprediction of the axial solids velocity in the tube center is balanced by an overprediction in the wall region to satisfy the imposed solids mass flux. Furthermore, the observed underprediction of the lateral solids segregation should also be compensated by an overprediction of the axial solids velocity in the neighborhood of the tube wall. However, the overprediction of the axial solids velocity in the wall region is not very pronounced as can be seen in Figure 7. Since no experimental data are available close to the tube wall, it is difficult to make a thorough comparison in this region. Moreover, small changes in the solids concentration or axial solids velocity in the outer region of the cross-sectional area strongly influence the integral solids mass flux.

The radial distribution of the kinetic fluctuation energy, characterized by θ, is shown in Figure 8. Higher values for the pseudo temperature in the tube center are obtained using the constitutive relations of Ding and Gidaspow ($\theta = 34$ m²·s^{-2}) compared to the results obtained by using the constitutive relations proposed in this work ($\theta = 11$ m²·s^{-2}). Higher values for the particulate phase shear viscosity using the latter relations ($\mu_s = 1$–5 Pa·s) compared to values obtained using the relations of Ding and Gidaspow ($\mu_s = 0.01$–0.5 Pa·s) enhance the radial transport of kinetic fluctuation energy, resulting in a flatter pseudo temperature profile.

In Figures 9 and 10 the calculated radial profiles of the axial gas velocity and axial slip velocity (i.e., difference be-
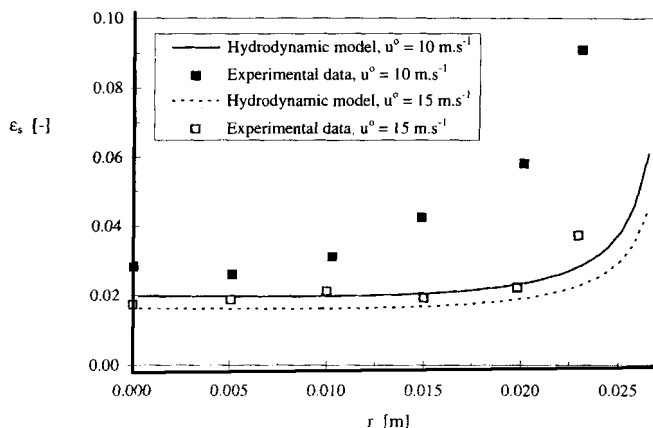
tween gas velocity and solids velocity) are respectively shown. In general, theoretically calculated slip velocities using the constitutive relations derived in this work show a better agreement with experimentally determined slip velocities (Yang et al., 1992) which roughly equal 5 to 8 times the terminal velocity of a single particle (0.79 m·s^{-1}). Using the relations proposed by Ding and Gidaspow, the calculated slip velocities are approximately two times the value of the terminal velocity. In the latter situation radial momentum transport is dominated by gas-phase turbulence, causing the observed maximum near the tube wall as reported by Nieuwland et al. (1994). This phenomenon cannot be observed in the slip velocity profile in case the relations derived in this work are used which is due to the dominant contribution to radial momentum transfer of the kinetic transport mechanism in the particulate phase.

The relations proposed by Ding and Gidaspow lead to a better agreement between calculated and experimentally observed axial pressure gradient. Applying the relations pre-
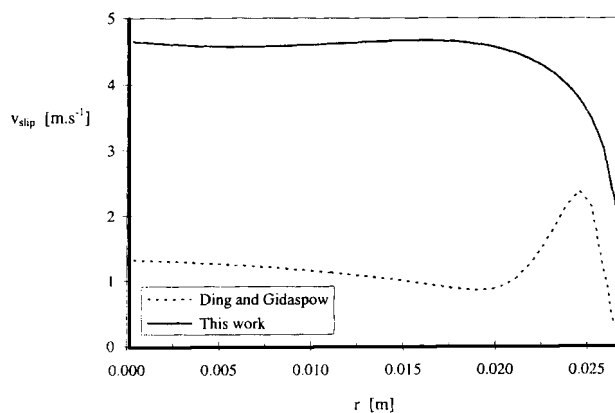
Figure 10. Calculated axial slip velocity as a function of the radial position at 2.5 m above the solids entry.

$R = 0.027$ m, $u^o = 14.4$ m·s^{-1}, $G_s = 350$ kg·m^{-2}·s^{-1}, $d_p = 129$ μm, $\rho_s = 2,540$ kg·m^{-3}.
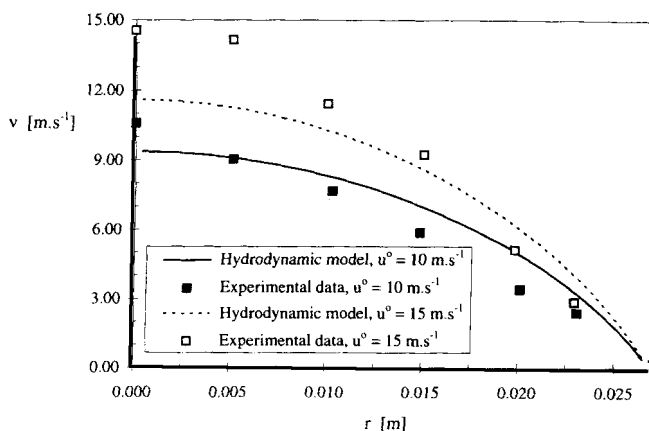
Figure 11. Calculated and experimentally determined solids concentration as a function of the radial position at 2.5 m above the solids entry for two gas velocities.

$R = 0.027$ m, $G_s = 300$ kg·m^{-2}·s^{-1}, $d_p = 129$ μm, $\rho_s = 2{,}540$ kg·m^{-3}.

locity, the theoretical results show a decrease in solids concentration and an increase in solids velocity, which is in qualitative agreement with experimental data. As discussed before, the model underestimates the lateral solids segregation, while the axial solids velocity is underestimated near the tube wall and overestimated in the tube center. The solids concentration is seriously underestimated over the entire tube radius for the case of $u^o = 10$ m·s^{-1}. By comparing the overall solids mass flux, obtained by averaging the experimentally determined local solids mass flux over the cross-sectional area, with the imposed solids mass flux shows $+20\%$ error indicating the inaccuracy of the measuring technique. On the other hand, the discrepancy can possibly be attributed to interaction between particle motion and gas-phase eddies and/or clustering behavior of the particles, phenomena both not accounted for in the model. It should be noticed, however, that the present hydrodynamic model contains no adjustable parameters which makes the correspondence between theory and experiments quite reasonable.

Theoretically calculated results have also been compared with experimental data reported by Bader et al. (1988). These authors investigated CFB hydrodynamics in a 10-m tall riser tube, with 30.4-cm internal diameter, operated with air as fluidizing agent and FCC ($d_p = 76$ μm, $\rho_s = 1{,}714$ kg·m^{-3}) as the particulate phase.

Figure 13 shows a comparison between the theoretically calculated and experimentally determined solids concentration profile for a superficial gas velocity u^o of 3.7 m·s^{-1} and a solids mass flux G_s of 98 kg·m^{-2}·s^{-1}, while in Figure 14 corresponding axial solids velocity profiles are shown. Again, both the constitutive relations for μ_s and κ proposed by Ding and Gidaspow and the relations proposed in this work have been used to obtain the theoretically calculated profiles shown in Figures 13 and 14. In the tube center the differences between the results obtained by applying these two groups of constitutive relations are small in comparison with the differences obtained in the 5.36-cm-dia. riser, discussed before. This can be attributed to the augmented importance of gas-phase turbulence due to the larger tube diameter (Eq. 9) as evident from Figure 15 which shows the individual contribu-

sented in the present study results in an overestimate of the axial pressure gradient by almost a factor of 4. This discrepancy might be attributed to a difference between the calculated solids velocity profile compared to the experimentally determined solids velocity profile near the tube wall, which influences the momentum exchange with the tube wall.

In addition, the effect of both solids mass flux and superficial gas velocity have been examined, using the constitutive relations proposed in this work. Calculations with increasing solids mass flux for constant superficial gas velocity resulted in increasing solids concentrations, while the velocity profiles were relatively unaffected. These results are in accordance with experimental data (Nieuwland et al., 1996).

Figures 11 and 12 show a comparison between calculated and experimentally determined solids concentration and axial solids velocity respectively, for two superficial gas velocities ($u^o = 10$ m·s^{-1}, $u^o = 15$ m·s^{-1}) at the same solids mass flux ($G_s = 300$ kg·m^{-2}·s^{-1}). With increasing superficial gas ve-
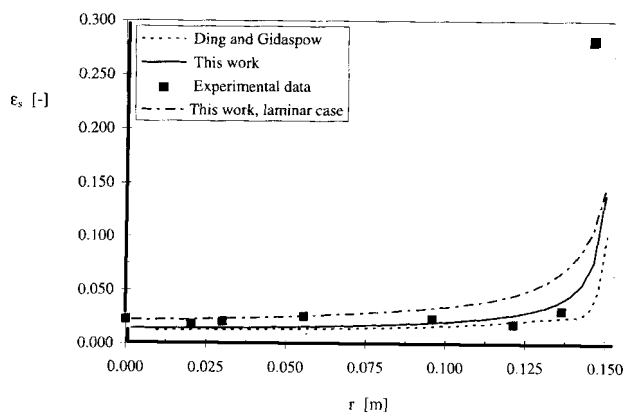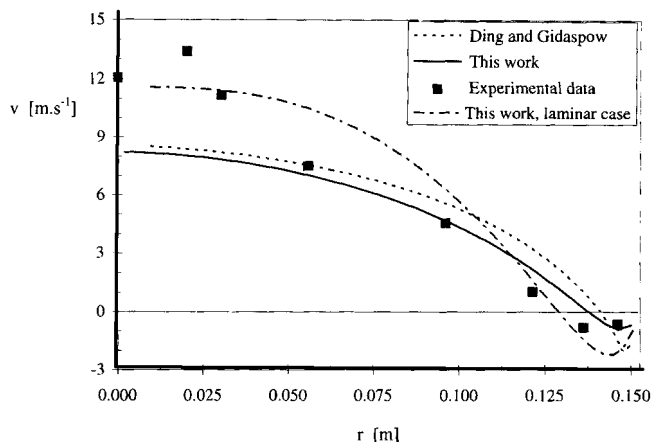

Figure 12. Calculated and experimentally determined axial solids velocity as a function of the radial position at 2.5 m above the solids entry for two gas velocities.

$R = 0.027$ m, $G_s = 300$ kg·m^{-2}·s^{-1}, $d_p = 129$ μm, $\rho_s = 2{,}540$ kg·m^{-3}.

Figure 13. Calculated and experimentally determined (Bader et al., 1988) solids concentration as a function of radial position at 9 m above the solids entry.

$R = 0.153$ m, $u^o = 3.7$ m·s^{-1}, $G_s = 98$ kg·m^{-2}·s^{-1}, $d_p = 76$ μm, $\rho_s = 1{,}714$ kg·m^{-3}.

Figure 14. Calculated and experimentally determined (Bader et al., 1988) axial solids velocity as a function of the radial position at 9 m above the solids entry.

$R = 0.153$ m, $u^o = 3.7$ m·s^{-1}, $G_s = 98$ kg·m^{-2}·s^{-1}, $d_p = 76$ μm, $\rho_s = 1,714$ kg·m^{-3}.

tions to the apparent viscosity of the gas-solid mixture. The radial momentum transport by the particulate phase is of minor importance in case the relations proposed by Ding and Gidaspow are applied, while the use of the relations derived in this work results in equal contributions of both phases.

In this case both models predict a small maximum in the radial profile for slip velocity which is due to the enhanced influence of gas-phase turbulence as explained before.

The calculated particulate phase shear viscosity near the tube wall ($\mu_s = 0.13$ Pa·s) corresponds better to the experimental value of the 0.7 Pa·s for this situation (Gidaspow et al., 1989), in comparison to the value obtained using the relations of Ding and Gidaspow ($\mu_s = 0.03$ Pa·s). Both models predict solids down flow near the tube wall (Figure 14), which

Figure 15. Calculated apparent bed viscosity, composed of several contributions, as a function of the radial position at 9 m above the solids entry.

$R = 0.153$ m, $u^o = 3.7$ m·s^{-1}, $G_s = 98$ kg·m^{-2}·s^{-1}, $d_p = 76$ μm, $\rho_s = 1,714$ kg·m^{-3}.

is in agreement with experimental data. However, due to overestimation of the solids velocity near the wall, both models underpredict the axial solids velocity in the tube center.

For the purpose of reference, the results of a calculation in which the gas-phase turbulence has been neglected is included in Figures 13 and 14. In this calculation the constitutive relations for μ_s and κ proposed in the present study were used. As evident from Figure 13 for the laminar case, the solids concentration increases over the entire tube radius where the deviation between theoretical predictions and experimental data becomes more pronounced near the tube wall.

The radial profile of the axial solids velocity changes considerably, as can be seen from Figure 14. The agreement between theory and experiment improves in the tube center; however, near the tube wall the solids downflow is overpredicted considerably.

Conclusion

A 2-D model based on the two fluid concept has been developed to quantitatively describe hydrodynamic key features prevailing in (dense) gas-solid two-phase flow. In literature the experimentally reported lateral solids segregation has been attributed to direct collisional interactions between particles and additionally to interaction between gas-phase eddies and dispersed particles (Sinclair and Jackson, 1989; Louge et al., 1991). Because no theory is yet available to model the interaction between gas-phase eddies and dispersed particles, turbulence has been modeled on a macroscopic scale using a modified Prandtl mixing length model. To model the influence of direct particle-particle collisions, the KTGF has been applied, based on the Chapman-Enskog theory of dense gases. In this theory it has been assumed that the gas-solid two-phase flow approximates the Maxwellian state (i.e., steady-state equilibrium conditions), which is not valid for riser flow. Deviation from this equilibrium condition has been accounted for using a first-order perturbation theory. Hereby the work of Ding and Gidaspow (1990), who adopted the Maxwell velocity distribution function, has been extended. Calculations without using the KTGF failed to describe the experimentally observed lateral solids segregation.

To validate the theoretical results the CFB hydrodynamics has been studied experimentally in a cold flow test unit. To obtain radial distributions of solids concentration and axial solids velocity, a reflective optical probe has been developed which is based on the same principle as the one used by Hartge et al. (1988).

Comparison of theoretically calculated results and experimental data show a satisfactory degree of agreement, especially when it is kept in mind that the model contains no adjustable parameters. However, the model slightly underpredicts the lateral solids segregation and yields an axial solids velocity profile with a more pronounced parabolic shape in comparison with its experimental counterpart.

A comparison of the results obtained by applying the constitutive relations proposed by Ding and Gidaspow (1990) and the relations derived in this study demonstrate the significance of the kinetic transport mechanism in the particulate phase. This transport mechanism has not been correctly modeled by Ding and Gidaspow applying the Maxwell velocity distribution function. This difference is of less significance in
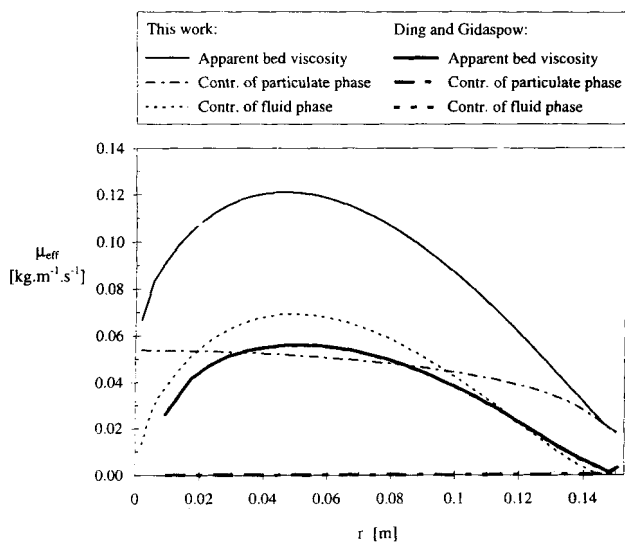
case gas-phase turbulence constitutes an important (radial) momentum transport mechanism.

In future work the microscopic interaction between gas-phase eddies and dispersed particles need to be considered in more detail.

Notation

d_p = particle diameter, m
g = gravitational force per unit mass, m·s^{-2}
g = radial distribution function
I = unit tensor
k = unit vector
n = number of particles per unit volume, m^{-3}
p = particulate phase momentum stress tensor, kg·m^{-1}·s^{-2}
R = tube radius, m
r = position vector, m
r = radial coordinate, m
δr = radial dimension of computational cell, m
δt = time step in numerical solution procedure, s
u = gas velocity, interstitial, m·s^{-1}
W = solids hold up, kg
δz = axial dimension of computational cell, m
z = axial coordinate, m

Greek letters

γ = dissipation due to inelastic mutual particle collisions, kg·m^{-1}·s^{-3}
ϵ = volume fraction
θ = pseudo particle temperatures, m^2·s^{-2}

Subscripts

mf = minimum fluidization
r = radial component

Superscripts

$'$ = after collision
c = collisional transport
(i) = ith-order approximation
k = kinetic transport
t = turbulence
T = transposed

Operators

D/Dt = substantial time derivative
$\partial/\partial r$ = spatial gradient
$\partial/\partial C$ = fluctuation velocity gradient
∂_e/∂_t = time derivative due to particle encounters
$:$ = scalar product of two tensors
$\cdot$ = scalar product of two vectors
$\sim$ = ensemble averaging
$\stackrel{\circ}{=}$ = traceless symmetric tensor

Literature Cited

Alder, B. J., and T. E. Wainwright, "Studies in Molecular Dynamics II: Behaviour of a Small Number of Elastic Spheres," *J. Chem. Phys.*, **33**, 1439 (1960).

Anderson, T., and R. Jackson, "A Fluid Mechanical Description of Fluidized Beds," *Ind. Eng. Chem. Fund.*, **6**, 527 (1967).

Bader, R., J. Findlay, and T. M. Knowlton, "Gas/Solids Flow Patterns in a 30.5 cm Diameter Circulating Fluidised Bed," *Circulating Fluidised Bed Technology: II*, P. Pasu and J. F. Large, eds., Pergamon Press, New York, p. 123 (1988).

Berker, A., and T. J. Tulig, "Hydrodynamics of Gas-Solid Flow in a Catalytic Cracker," *Chem. Eng. Sci.*, **41**, 821 (1986).

Chapman, A., and T. G. Cowling, "The Mathematical Theory of Non-Uniform Gases," 3rd ed., Cambridge Univ. Press, Cambridge (1970).

Deissler, R. G., NACA-Report 1210 (1955).

Ding, J., and D. Gidaspow, "A Bubbling Fluidisation Model Using Kinetic Theory of Granular Flow," *AIChE J.*, **36**, 538 (1990).

Dry, R. J., "Radial Concentration Profiles in a Fast Fluidised Bed," *Powder Technol.*, **49**, 37 (1986).

Gidaspow, D., Y. P. Tsuo, and K. M. Luo, "Computed and Experimental Cluster Formation and Velocity Profiles in Circulating Fluidized Beds," *Fluidization VI*, J. R. Grace, L. W. Shemilt and M. A. Bergougnou, eds., p. 81 (1989).

Hartge, E. U., D. Rensner, and J. Werther, "Solids Concentration and Velocity Patterns in Circulating Fluidised Beds," in *Circulating Fluidised Bed Technology: II*, P. Basu and J. F. Large, eds., Pergamon Press, p. 165 (1988).

Jenkins, J. T., and S. B. Savage, "A Theory for the Rapid Flow of Identical, Smooth, Nearly Elastic, Spherical Particles," *J. Fluid Mech.*, **130**, 187 (1983).

Kuipers, J. A. M., "A Two Fluid Micro Balance Model of Fluidized Beds," PhD Diss., Twente Univ., Enschede, The Netherlands (1990).

Kuipers, J. A. M., W. Prins, and W. P. M. van Swaaij, "Theoretical and Experimental Bubble Formation at a Single Orifice in a Two-Dimensional Gas Fluidised Bed," *Chem. Eng. Sci.*, **46**, 2881 (1991).

Kuipers, J. A. M., K. J. van Duin, F. P. H. van Beckum, and W. P. M. van Swaaij, "A Numerical Model of Gas Fluidized Beds," *Comput. Chem. Eng.*, **17**, 839 (1993).

Kwauk, M., W. Ningde, Y. Li, C. Bingyu, and S. Zhiyan, "Fast Fluidization at ICM," *Circulating Fluidized Bed Technology: I*, P. Basu, ed., Pergamon Press, p. 33 (1986).

Louge, M. Y., E. Mastorakos, and J. T. Jenkins, "The Role of Particle Collisions in Pneumatic Transport," *J. Fluid Mech.*, **231**, 345 (1991).

Lun, C., S. B. Savage, D. J. Jeffrey, and N. Chepurniy, "Kinetic Theories for Granular Flow: Inelastic Particles in Couette Flow and Slightly Inelastic Particles in a General Flow Field," *J. Fluid Mech.*, **140**, 223 (1984).

Ma, D., and G. Ahmadi, "An Equation of State for Dense Rigid Sphere Gases," *J. Chem. Phys.*, **84**, 3449 (1986).

Miller, A., and D. Gidaspow, "Dense Vertical Gas Solid Flow in a Pipe," *AIChE J.*, **38**, 1801 (1992).

Nieuwland, J. J., P. Roos, J. A. M. Kuipers, and W. P. M. van Swaaij, "Hydrodynamic Modelling of Circulating Fluidised Beds," AIChE Meeting, Atlanta (Apr., 1994).

Nieuwland, J. J., P. Huizenga, J. A. M. Kuipers, and W. P. M. van Swaaij, "Hydrodynamic Modelling of Circulating Fluidised Beds," *Chem. Eng. Sci.*, **49**, 5803 (1994).

Nieuwland, J. J., J. A. M. Kuipers, and W. P. M. van Swaaij, "Measurement of Solids Concentration and Axial Solids Velocity in Dense Gas-Solid Two-Phase Flows," *Powder Technol.* **77**, 127 (1996).

Nieuwland, J. J., "Hydrodynamic Modelling of Gas-Solid Two-Phase Flows," PhD Diss., Twente Univ., Enschede, The Netherlands (1995).

Ogawa, S., A. Umemura, and N. Oshima, "On the Equations of Fully Fluidized Granular Materials," *J. Appl. Math. Phys.*, **31**, 483 (1980).

Patankar, S. V., *Numerical Heat Transfer and Fluid Flow*, Hemisphere (1980).

Pita, J. A., and S. Sundaresan, "Gas Solid Flow in Vertical Tubes," *AIChE J.*, **37**, 1009 (1991).

Pita, J., and S. Sundaresan, "Developing Flow of a Gas-Particle Mixture in a Vertical Riser," *AIChE J.*, **39**, 541 (1993).

Schiller, L., and A. Naumann, "Über die grundlegenden Berechnungen bei der Schwerkraftaufbereitung," *Z. Ver. Dtsch. Ing.*, **77**, 318 (1935).

Sinclair, J., and R. Jackson, "Gas-Particle Flow in a Vertical Pipe with Particle-Particle Interactions," *AIChE J.*, **35**, 1473 (1989).

Tsuji, Y., Y. Morikawa, and H. Shiomi, "LDV Measurements of an Air-Solid Flow in a Vertical Pipe," *J. Fluid Mech.*, **139**, 417 (1984).

Wen, Y. C., and Y. H. Yu, "Mechanics of Fluidization," *AIChE Symp. Ser.*, **62**, 100 (1966).

Yang, Y. L., Y. Yin, Z. Q. Yu, and Z. W. Wang, "Investigation on Slip Velocity Distributions in the Riser of Dilute Circulating Fluidized Beds," *Powder Technol.*, **73**, 67 (1992).

Yerushalmi, J., and A. A. Avidan, "High Velocity Fluidization," in *Fluidization*, Chap. 7, J. F. Davidson, R. Clift, and D. Harrison, 2nd ed., Academic Press, New York, p. 225 (1985).